INDERSCIENCE PUBLISHERS
Linking academia, business and industry through research

International Journal of Manufacturing Technology and Management

ISSN online: 1741-5195 - ISSN print: 1368-2148
https://www.inderscience.com/ijmtm

Mathematical modelling and numerical simulation of direct extrusion process for different cross-section of dies

D.P. Jena

Article History:

Received:	01 March 2019
Accepted:	19 January 2021
Published online:	19 May 2023

Copyright © 2023 Inderscience Enterprises Ltd.

Mathematical modelling and numerical simulation of direct extrusion process for different cross-section of dies

D.P. Jena

Department of Industrial Design,
National Institute of Technology Rourkela,
769008, India
Email: jena.dibya@gmail.com

Abstract: The present research derives the analytical solutions for direct extrusion for different cross-sections of dies. Additionally, to exterminate the limitation and complexity of analytical solution for complex shapes, and validation of analytically calculated results, the finite element-based simulation is demonstrated. First, the tensile and compressive strength for AA6063-T7 and AA6061 are calculated using simulations and verified with experimental measurements. Then, the simulation of direct extrusion is conducted and authenticated with experimental measurements. Finally, with convinced assumptions, the analytical model for different dies such as elliptical, square, and rectangle shapes are derived. It is shown that the calculated results from simulations agree to analytically calculated results with less than 5% error for different coefficient of frictions and different extrusion ratios.

Keywords: tensile test; compressive test; analytical modelling; direct extrusion process; finite element analysis; FEA.

Reference to this paper should be made as follows: Jena, D.P. (2023) 'Mathematical modelling and numerical simulation of direct extrusion process for different cross-section of dies', *Int. J. Manufacturing Technology and Management*, Vol. 37, No. 1, pp.49–70.

Biographical notes: D.P. Jena is presently acting as an Assistant Professor at NIT Rourkela and completed his PhD in 2015 from IIT Bhubaneswar. His expertise areas are sound, vibration, metamaterials and manufacturing.

1 Introduction

In general, the objective of any industry is to manufacture a product or component cost effectively, however, maintaining desired quality consistently. With the intention to achieve such goals, one should opt established methods for selecting material, manufacturing processes which lead to final product including every sub-steps. Out of all manufacturing process, the forming processes are always preferred for low waste and high surface finish. The extrusion process is the one, where continuous production can happen for a constant cross-section without any waste. However, the disadvantage of this process is its limitation to few cross-sections only and inability to withstand to thermo-mechanical stresses (Dieter, 2013; Bauser et al., 2006). For more details, one can

Copyright © 2023 Inderscience Enterprises Ltd.

refer literature (Dieter, 2013; Ghosh and Mallik, 2010). However, a brief review is presented successively.

Quenzi et al. (1972) proposed analytical solution for lateral extrusion process. In said model, he had implemented strain hardening with the help of slip line mechanism. In recent times, Bagherpour et al. (2015) have suggested a new method in extruding the billet over linear die by undergoing shear deformation. Same authors have also demonstrated a detailed methodology to optimise the inclination angle by applying different boundary conditions on inlet. In a similar way, Haghighat and Askar (2015) have demonstrated the bimetal extrusion through conical die using upper bound technique. They investigated analytically different parameters which influence the process and validated numerically. In parallel, Tabatabaei et al. (2015) have proposed a novel methodology which is in principle of electrical analogies of direct extrusion process followed by experimental agreements.

The most accurate method for optimising the extrusion process and influencing parameters is through experimentations which is expensive. In same line and length, Yermanok (1997) had presented the analytical and experimental relationships to optimise the parameters, such as billet length relation to billet diameter, metal flow relationship as a function of maximum force and L/D ratio, in extrusion process. Similarly, Saboori et al. (2006) conducted experimental investigations for forward and backward extrusion using an optimal conical and a curved die profile and had reported that the energy consumption is more in conical die than curved die. Likewise, Chaudhari et al. (2012) have demonstrated experimentally the role of die angle for aluminium. They found that the hardness and the observed surface finish on the surface highly depend on die angle and the optimal one is around 450. In recent years, Comaneci et al. (2015) in their experiments on combining circular to rectangle direct extrusion and equal angular pressing came to conclusion that the combined procedure is capable to enhance the mechanical properties of the billet significantly.

In recent years, finite element analysis, known as FEA, is extensively chosen to evaluate the design or process parameters. Chanda et al. (2000) had first shown the potential of FEA in simulating the direct extrusion process using aluminium alloy using DEFORMTM. Abrinia and Makaremi (2009) reported novel FEA method which is based on solving energy equations for spread extrusion for different cross-section of die, which agree to experimental investigations. Subsequently, Plančak et al. (2009) have also investigated extruded force for a non-axisymmetric backward extrusion of aluminium and steel billets using non-circular punch and reported the adequate agreement between numerical and experimental results. Substantial research has been conceded to simulate the extrusion process using finite element method with subsequent possible experimental investigation (Plančak et al., 2009; Bressan et al., 2014). However, such attempts are limited to the same billet and die cross-section. Such limitations have been addressed by Oyinbo et al. (2005). Ryzinska and Gieleta (2016) have investigated numerically and experimentally the backward extrusion process to fabricate impact energy-absorbing device. In recent times, Pahlevanpour et al. (2018) have experimentally investigated the extrusion of ZK60 and estimate the directional quasi-static and strain-controlled characteristics of fatigue using stress-strain hysteresis loops. Nouri et al. (2018) have demonstrated the possibility of twist extrusion by embedding a channel in direct extrusion followed by the twist zone using FEA and experimental investigations. Nevertheless, few researchers (Bryan et al., 2017; Zhang et al., 2018) have also demonstrated the potential of computational fluid dynamics (CFD) in simulating direct

extrusion process and metal flow behaviour. Summarising, the challenge of simulating extremely large deformation adequately still remains as a challenge and need next level of improvement.

From literature review, it can be inferred that the analytical solution for different shapes of dies have not been addressed sufficiently. Moreover, a detailed investigation using FEM is essential to overcome the lacuna of mathematical complexities which exponentially increase over shapes. The present research first tried to establish the benchmarking simulations which are compared with experimental measurements. Subsequently, the analytical solutions are derived for various shapes such as rectangular, square, and elliptical shapes. The analytical solutions are examined against numerical simulations. Moreover, the role of friction and different material properties are also investigated to substantiate the analytical solutions.

2 Finite element modelling

The problem in hand has objective to derive analytical solution for extrusion process having different cross-section of dies. In order to augment the research a numerical simulation is found indispensable. So, the numerical simulations including benchmarking validations are conducted in ANSYS® platform. The desired geometry and corresponding mesh are generated before simulation. Moreover, the various crucial parameters such as contact modelling, material properties modelling, suitable element selection including corresponding parameters definitions, and finally solver configurations are addressed appropriately. However, the desired simulation involves very large deformation. Henceforth, the dynamic meshing and corresponding definition of re-meshing are considered in finite element formulation.

First, the simulations are conducted to estimate the tensile and compressive test of aluminium alloys which are AA6063-T7 and AA6061, respectively. Next, the benchmarking simulation of an extrusion process is done with aluminium 5,154. The calculated results are validated with reports available in literature. The material properties of said materials can be found in literature (George et al., 2004; Khlystov et al., 2013). For simulation, the Armstrong and Frederick model (Sinaie, 2009; Frederick and Armstrong, 2007) is used to model the material behaviour.

The corresponding mathematical formulation may be written as mentioned:

$$\alpha = \sum_{i=1}^{n} \alpha_i \text{, where } \dot{\alpha}_i = \frac{2}{3} C_i \dot{\varepsilon}^{pl} - \alpha \gamma_i \dot{\bar{\varepsilon}}^{pl} \text{ ssss} \tag{1}$$

where

n Back stress components.

$\dot{\varepsilon}^{pl}$ Plastic strain rate.

α Back stress

$\dot{\alpha}_i$ The back stress rate of i^{th} component.

$\dot{\bar{\varepsilon}}^{pl}$ Plastic strain rate.

C_i and γ_i Plastic modulus and corresponding data history.

Figure 1 Curve fitting; (a) tensile, and (b) compression test

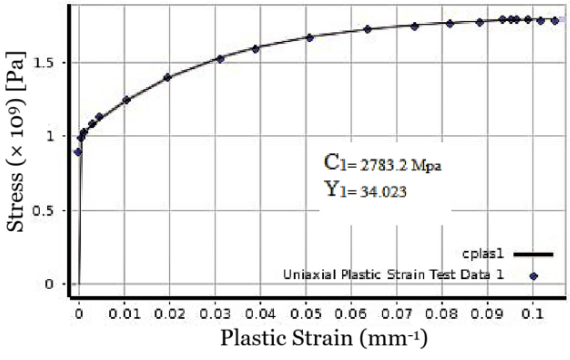

(a)

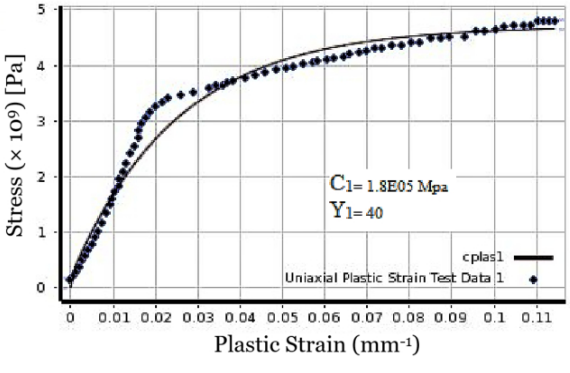

(b)

As the simulation involves extremely large deformation, the desired finite element formulation for initialisation followed by integration of dynamic re-meshing are found obligatory and are taken care in all simulations. The role of adequate element selection is observed to be crucial in achieving desired numerical stability.

The virtual work based finite element model can be written as (Bonet and Wood, 2008; Gadala and Wang, 1999):

$$\int_v \sigma_{ij}\delta e_{ij}dV = \int_v f_i^B \delta u_i dV + \int_s f_i^s \delta u_i ds \tag{2}$$

where

σ_{ij} Cauchy stress component.

$e_{ij} = \frac{1}{2}\left(\frac{\partial u_i}{\partial x_j} + \frac{\partial u_j}{\partial x_i}\right)$ [Deformation tensor (Bathe, 1982)].

u_i and x_i Displacement, and current coordinate.

f_i^B Body force components.

f_i^s Surface traction.

V and s Volume and surface of deformed body.

On differentiating equation (2) the desired finite element model can be obtained. Moreover, the corresponding desired Cauchy stress, which is assessed by using below mathematical formulation (McMeeking and Rice, 1975).

$$\dot{\sigma}_{ij}^{j} = \dot{\underset{ij}{\sigma}} - \sigma_{ik}\,\dot{\underset{jk}{\omega}} - \sigma_{jk}\,\dot{\underset{ik}{\omega}} \tag{3}$$

where

$\dot{\sigma}_{ij}^{j}$ Jaumann rate of Cauchy stress.

$\dot{\underset{ij}{\omega}}$ Spin tensor $\left(\frac{1}{2}\left(\frac{\partial v_i}{\partial x_j} - \frac{\partial v_j}{\partial x_i}\right)\right)$

$\dot{\underset{ij}{\sigma}}$ Time dependent Cauchy stress.

Furthermore, the stress used to be changed with respect to corresponding strain and can be stated as:

$$\dot{\sigma}_{ij}^{j} = c_{ijkl} d_{kl} \tag{4}$$

c_{ijkl}, v_i Material constitutive tensor and velocity, respectively.

$d_{ij} = \frac{1}{2}\left(\frac{\partial v_i}{\partial x_j} + \frac{\partial v_j}{\partial x_i}\right)$ (Rate of deformation tensor).

As the large deformation simulation is desired to simulate the problem in hand, the adequate finite element formulation is essential. In present case, the mixed $u - p$ formulation is observed appropriate and is opted to estimate the rate of change in volume on applied load (Bathe, 1982). However, the implementation of dynamic re-meshing is indispensable for such simulation. Moreover, the desired criteria to re-mesh the deformed mesh in time domain simulation is critical and is tuned in simulating benchmark simulations. In order to have detailed understanding, one can refer literature (Onate et al., 2004).

The mathematical equation used in FEA to compute the stiffness and body force can be written as (Zienkiewicz, 1967).

$$[K]\{u\} = \{F^a\} + \{F^r\} \tag{5}$$

where

$[K] = \sum_{m=1}^{N} [k_e]$ Stiffness matrix.

$\{u\}$ Nodal displacement vector.

N No of elements.

$[K_e]$ Stiffness matrix.

$\{F^r\}$ Reaction load vector.

The load, $\{F^a\}$, can be stated in vector form as:

$$\{F^a\} = \{F^{nd}\} + \{F^{ac}\} + \sum_{m=1}^{N} \left(\{F_e^{th}\} + \{F_e^{pr}\} \right) \tag{6}$$

where

$\{F^{nd}\}$ Nodal load vector.

$\{F^{ac}\} = -[M]\{a_c\}$ Acceleration vector.

$[M] = \sum_{m=1}^{N} [M_e]$ [M] Total mass matrix.

$[M_e]$ Element mass matrix.

$\{a_c\}$ Acceleration vector.

$\{F_e^{th}\}$ Thermal element.

$\{F_e^{pr}\}$ Load vector.

3 Benchmarking and validation

Benchmarking simulation is found indispensable in order to augment the proposed research. To start with, first, both tensile test and compressive test are investigated for aluminium alloy AA6063-T7 and AA6061. For simulation, the experimentally measured tensile and compressive test data are used to define accurate material properties (George et al., 2004; Khlystov et al., 2013).

3.1 Tensile test and compression test

The tensile test and compressive test are numerically simulated by mimicking the ASTM E8/E8M-16a, and ASTM E9-09 standards, respectively. The complete simulation including modelling and meshing are done in ANSYS® platform. The finite element discretisation is done using surface-156 and Solid-285 element, correspondingly. Total 904 nodes and 790 elements are generated for tensile testing and 634 nodes and 2104 elements are generated for compression testing. Both the elements support dynamic re-meshing and are applied on nonlinear zones in geometry. The desired boundary loading conditions are incorporated in simulation, similar to actual environment. For example one end is made stationary by defining zero degree of freedom and at other end desired loads are applied. The static solver with 100 steps is used to calculate the Von Mises stress and plastic strain across the geometry. On reaching the steady state solution, the obtained results are shown in Figures 2(a) and 2(b), correspondingly.

From estimated results shown in Figure 2, one can notice that the simulation results approve experimentally reported results (George et al., 2004; Khlystov et al., 2013)

extensively. From this the robustness of the proposed simulations is established. Moreover, to illustrate the reliability of simulation, the exclusive grid testing is also conducted. The demonstrated simulations include exceptionally large deformation and therefore the dynamic re-meshing is incorporated. So in these scenarios, rather than the fine re-meshing, the dynamic re-meshing criteria setting is found more crucial and one should tune it with respect to number of steps involved in steady state solution configuration. The default fine meshing is found suitable with proper tuning of re-meshing criteria. The computational requirement is not found significant and can be mentioned as that the demonstrated solution was achieved by using a HP-Elite desktop (processor speed 3.40 GHz, i7 processor, and 16 GB RAM) in ≈ 10 minutes.

Figure 2 Experimental validation, (a) tensile, and (b) compression test

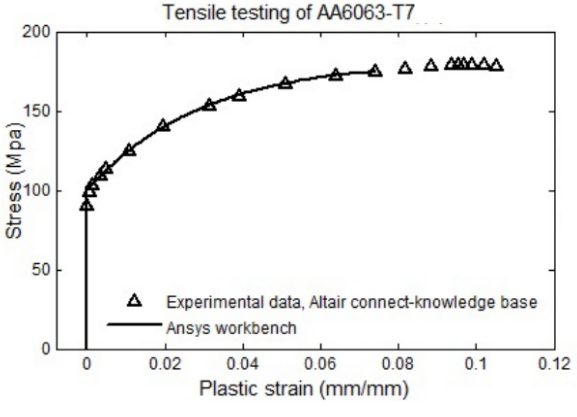

(a)

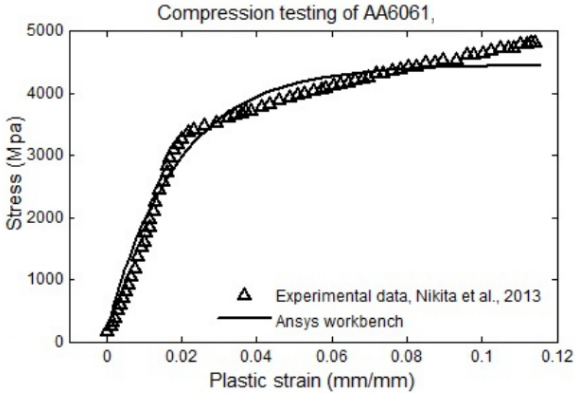

(b)

3.2 Simulating direct extrusion process

Next, the benchmarking simulation of direct extrusion process is conducted. Following literature (Noorani-Azad et al., 2005), the geometry is created in design-modeller followed by finite element meshing using Solid-285 element. Total generated 1,056

nodes and 1,573 elements are used for investigation of a cold extrusion process. As mentioned earlier the geometry is assigned as adaptive zone which supports dynamic re-meshing criteria. Similar to earlier simulations, the applied loads on boundaries are applied to mimic the executed experiment. The die is made rigid by assigning zero degree of freedom and the sought after boundary loads are applied on the other side of the surface of the billet. Similar to earlier analyses, the static analysis solver is used for investigation. The estimated numerical result over lapped with experimentally measured data (Noorani-Azad et al., 2005) and are shown in Figure 3. From figure, one can notice that the estimated result agrees to experimental measured data adequately. From this, it can be perceived that the proposed simulation technique is consistent and robust enough to augment the proposed research such as validation of analytically calculated results for different shapes of dies. Other factors such as dynamic re-meshing criteria and contacts between die and billet are already discussed to achieve said result.

Figure 3 Experimental validation of direct extrusion simulation

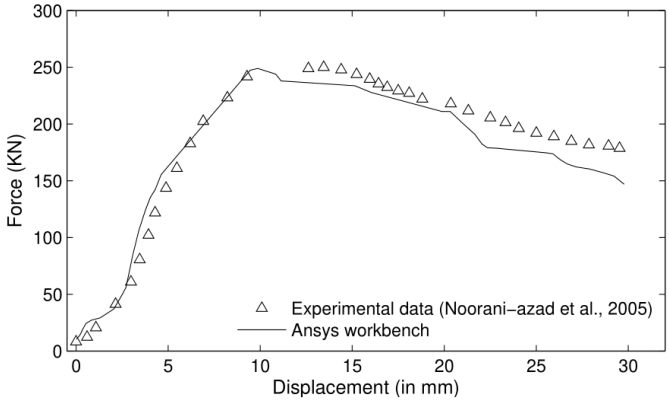

4 Analytical modelling of direct extrusion process

The analytical solutions are most cost effective solution in designing. In present research, the analytical solution for different shapes of die are derived by taking reference of known solution for circular cross-section (Bauser et al., 2006; Ghosh and Mallik, 2010) and are explained in following sub-sections.

4.1 Elliptical cross-section

Assumptions: Since a constant sliding friction which exists between the billet and the die wall, the force balance on the cross-section are carried out where α is the semi-cone angle and a is the initial radius of the billet. The a_f is the final major radius, and b is the final minor radius of the billet. When $b = a_f$ then it becomes a circular cross-section instead of an ellipse. Back stress acting on the billet is zero.

The area of circle can be computed using πa^2 and the area of ellipse is πab. Stresses acting on elemental billet subject to the axis-symmetry of the extrusion using slab method are shown in Figure 4.

Figure 4 Schematic of stresses acting on unit-cross-section (slab method)

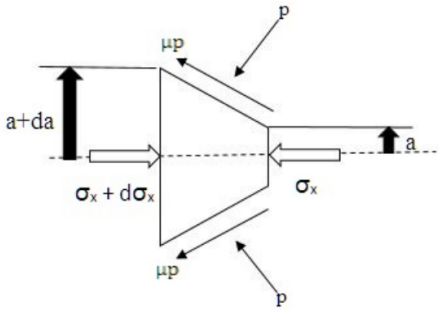

It can be noticed in Figure 4 that the σ_x is the required pressure for extrusion, where the μp is the frictional force among the billet and the die. The p is normal force applied on the billet and can be termed as applied stress. The slant surface area can be computed using below expression.

$$\frac{\pi(a+da)^2 - \pi ab}{\sin\alpha} \tag{7}$$

However, neglecting the smaller values and higher order terms, the aforementioned equation is reduced to:

$$\frac{\pi a^2 + 2\pi a da - \pi ab}{\sin\alpha} \tag{8}$$

Referring to Figure (4), now the equilibrium condition is applied. This can be defined is applied. This can be defined as net horizontal forces are zero and net vertical forces are also zero. The corresponding expressions are written as:

$$\begin{aligned}\sum H = 0 \rightarrow (\sigma_x + d\sigma_x)\pi(a+da)^2 - \sigma_x \pi ab \\ = (\mu p\cos\alpha + p\sin\alpha)\frac{\pi a^2 + 2\pi a da - \pi ab}{\sin\alpha}\end{aligned} \tag{9}$$

$$\sum V = 0 \rightarrow \mu p\sin\alpha - p\cos\alpha = 0 \Rightarrow \tan\alpha = {}^{1}\!/_{\mu} \tag{10}$$

The aforementioned equation (9), simplifying by neglecting smaller values and higher order terms, is re-written as:

$$\sigma_x \pi a^2 + 2\sigma_x \pi a da + d\sigma_x \pi a^2 - \sigma_x \pi ab = (\mu p\cot\alpha + p)(\pi a^2 + 2\pi a da - \pi ab) \tag{11}$$

Now, dividing with the area πa^2 on both sides, the equation becomes:

$$\sigma_x\left(\frac{a-b}{a}\right) + 2\sigma_x\frac{da}{a} + d\sigma_x = (\mu\cot\alpha + 1)\left(2p\frac{da}{a} + p\left(1 - \frac{b}{a}\right)\right) \tag{12}$$

On applying Trescas yield criteria (taking applied stress as positive and induced stress as negative), i.e., p is positive and σ_x is negative, the induced stress σ_x can be stated as:

$$-\sigma_x + p = y \Rightarrow p = \sigma_x + y \tag{13}$$

On substituting equation (13) in equation (12), the induced stress can be expressed as:

$$\sigma_x\left(\frac{a-b}{a}\right)+2\sigma_x\frac{da}{a}+d\sigma_x=(\mu\cot\alpha+1)\left(2(y+\sigma_x)\frac{da}{a}+(y+\sigma_x)\left(1-\frac{b}{a}\right)\right) \tag{14}$$

Again on simplifying, the $d\sigma_x$ can be expressed as:

$$\frac{d\sigma_x}{(y\mu\cot\alpha+\sigma_x\mu\cot\alpha+y)}=2\frac{da}{a}+\left(\frac{a-b}{a}\right) \tag{15}$$

Now, integrating the above equation on both sides:

$$\int\frac{d\sigma_x}{(y\mu\cot\alpha+\sigma_x\mu\cot\alpha+y)}=2\int\frac{da}{a}+\left(\frac{a-b}{a}\right) \tag{16}$$

$$\frac{\ln(y\mu\cot\alpha+\sigma_x\mu\cot\alpha+y)}{\mu\cot\alpha}=2\ln a+\left(1-\frac{b}{a}\right)+c \tag{17}$$

Note: For simplification, the term $\left(\frac{a-b}{a}\right)$ is taken as differential term.

At $a = a_f$, $\sigma_x = 0$, the above expressions become:

$$\frac{\ln(y\mu\cot\alpha+y)}{\mu\cot\alpha}=2\ln a_f+c \tag{18}$$

$$c=\frac{\ln(y\mu\cot\alpha+y)}{\mu\cot\alpha}-2\ln a_f \tag{19}$$

At steady state or end of the permanent deformation, the a will become a_f. So the term $\left(\frac{a-b}{a}\right)$ will become $\left(\frac{a_f-b}{a_f}\right)$. By putting $B = \mu \cot \alpha$ and substitute equation (19) in equation (17), the σ_x can be estimated as mentioned below:

$$\frac{\ln(B\sigma_x+(1+B)y)}{B}=2\ln a+\frac{(a_f-b)}{a_f}+\frac{\ln(y(1+B))}{B}-2\ln a_f \tag{20}$$

$$\ln\left(\frac{B\sigma_x+(1+B)y}{y(1+B)}\right)^{1/B}=\ln\left(\frac{a}{a_f}\right)^2+\frac{(a_f-b)}{a_f} \tag{21}$$

$$\sigma_x=\frac{y(1+B)}{B}\left(e^{B\left(\ln\left(\frac{a}{a_f}\right)^2+\frac{(a_f-b)}{a_f}\right)}-1\right) \tag{22}$$

Analytical results of extrusion pressure for different values of frictions are shown in Figure 5. The cross validation with respect to aforementioned numerical simulation are carried out in subsequent sections. The required force for extrusion is calculated by using $F=\frac{\pi}{4}d^2\sigma_x$ expression. Where F is the force necessary to extrude the material and d is the initial diameter of the billet.

4.2 Square cross-section

Assumptions: As discussed in earlier section, considering a constant sliding friction which exists between the billet and the die wall, the force balance on the cross-section is carried out where α is the semi-cone angle and a be the initial and a_f be the final side of the billet. Back stress acting on the billet is zero. The area of circle can be computed using πa^2 and the area of square = a^2. In this case the extrusion force has been calculated by $F = \frac{a^2}{\sigma_x}$ expression. Stresses acting on elemental billet subject to the axis-symmetric of extrusion using slab method are shown in Figure 4. It can again be noticed in Figure 4 that the σ_x is the required pressure for extrusion, where the μp is the frictional force among the die and billet. The slant surface area can be computed using below expression.

$$\frac{\pi(a+da)^2 - a^2}{\sin\alpha} \tag{23}$$

Neglecting the smaller values and higher order terms, aforementioned equation becomes:

$$\frac{\pi a^2 + 2\pi a da - a^2}{\sin\alpha} \tag{24}$$

Referring to Figure (4), now the equilibrium condition is applied. This can be defined as net horizontal forces are zero and net vertical forces are also zero. In line with aforementioned objective, the corresponding expressions may be written as:

$$\sum H = 0 \rightarrow (\sigma_x + d\sigma_x)\pi(a+da)^2 - \sigma_x a^2 = (\mu p\cos\alpha + p\sin\alpha)\frac{\pi a^2 + 2\pi a da - a^2}{\sin\alpha} \tag{25}$$

$$\sum V = 0 \rightarrow \mu p\sin\alpha - p\cos\alpha = 0 \Rightarrow \tan\alpha = {}^{1}\!/_{\mu} \tag{26}$$

On simplifying equation (25) by neglecting smaller values and higher order terms, the equation can also be re-written as:

$$\sigma_x\pi a^2 + 2\sigma_x\pi a da + d\sigma_x\pi a^2 - \sigma_x a^2 = (\mu p\cot\alpha + p)(\pi a^2 + 2\pi a da - a^2) \tag{27}$$

Now, dividing with the area πa^2 on both sides, the equation becomes:

$$\sigma_x\left(1-\frac{1}{\pi}\right) + 2\sigma_x\frac{da}{a} + d\sigma_x = (\mu\cot\alpha + 1)\left(2p\frac{da}{a} + p\left(1-\frac{1}{\pi}\right)\right) \tag{28}$$

As discussed earlier, on applying Trescas yield criteria (applied stress is positive and induced stress is negative), i.e., p is positive and σ_x will be negative, the induced stress σ_x can be stated as:

$$-\sigma_x + p = y \Rightarrow p = \sigma_x + y \tag{29}$$

On substituting equation (29) in equation (28), the induced stress can be expressed as:

$$\sigma_x\left(1-\frac{1}{\pi}\right) + 2\sigma_x\frac{da}{a} + d\sigma_x = (\mu\cot\alpha + 1)\left(2(y+\sigma_x)\frac{da}{a} + (y+\sigma_x)\left(1-\frac{1}{\pi}\right)\right) \tag{30}$$

Again on simplifying, the $d\sigma_x$ can be expressed as:

$$\frac{d\sigma_x}{\left(y\mu\cot\alpha+\sigma_x\mu\cot\alpha+y\right)}=2\frac{da}{a}+\left(1-\frac{1}{\pi}\right) \tag{31}$$

Integrating the above equation on both sides:

$$\int\frac{d\sigma_x}{\left(y\mu\cot\alpha+\sigma_x\mu\cot\alpha+y\right)}=2\int\frac{da}{a}+\left(1-\frac{1}{\pi}\right) \tag{32}$$

$$\frac{\ln\left(y\mu\cot\alpha+\sigma_x\mu\cot\alpha+y\right)}{\mu\cot\alpha}=2\ln a+\left(1-\frac{1}{\pi}\right)+c \tag{33}$$

Note: Here, for further simplification considering $\left(1-\frac{1}{\pi}\right)$ as differential term.

At $a = a_f$, $\sigma_x = 0$, the above expressions become:

$$\frac{\ln\left(y\mu\cot\alpha+y\right)}{\mu\cot\alpha}=2\ln a_f+c \tag{34}$$

$$c=\frac{\ln\left(y\mu\cot\alpha+y\right)}{\mu\cot\alpha}-2\ln a_f \tag{35}$$

By putting $B = \mu$ cot α and substitute equation (35) in equation (33), the σ_x can be estimated as mentioned below:

$$\frac{\ln\left(B\sigma_x+(1+B)y\right)}{B}=2\ln a+\left(1-\frac{1}{\pi}\right)+\frac{\ln(y(1+B))}{B}-2\ln a_f \tag{36}$$

$$\ln\left(\frac{B\sigma_x+(1+B)y}{y(1+B)}\right)^{1/B}=\ln\left(\frac{a}{a_f}\right)^2+\left(1-\frac{1}{\pi}\right) \tag{37}$$

$$\sigma_x=\frac{y(1+B)}{B}=\left(e^{B\left\{\ln\left(\frac{a}{a_f}\right)^2+\left(1-\frac{1}{\pi}\right)\right\}}-1\right) \tag{38}$$

Using aforementioned equations, the analytical solutions for different coefficient of friction are calculated and are shown in Figure 5. The cross validation using FEA-based simulations carried out in subsequent sections.

4.3 Rectangular cross-section

Assumptions: Similar to earlier section, again, considering a constant sliding friction which exists between the billet and the die wall, the force balance on the cross-section is carried out where α is the semi-cone angle and a initial radius of the billet. The a_f is the larger side of the rectangle and b be the smaller side of the rectangle. Back stress acting on the billet is zero.

The area of circle can be computed using πa^2 and the area of rectangle = ab. In this case the extrusion force is calculated by $F = \frac{ab}{\sigma_x}$ expression. In this context $a = a_f$ at the end of the process. Stresses acting on elemental billet subject to the axis-symmetric of extrusion are shown in Figure 4.

It can be noticed in Figure 4 that the σ_x is the required pressure for extrusion, where the μp is the frictional force among the die and billet. The slant surface area can be computed using below expression.

$$\frac{\pi(a+da)^2 - ab}{\sin\alpha} \tag{39}$$

The said equation can be written after neglecting higher order terms as:

$$\frac{\pi a^2 + 2\pi ada - ab}{\sin\alpha} \tag{40}$$

Referring to Figure (4), now the equilibrium condition is applied. This can be defined as net horizontal forces are zero and net vertical forces are also zero. This can be stated as:

$$\sum H = 0 \rightarrow (\sigma_x + d\sigma_x)\pi(a+da)^2\sigma_x ab = (\mu p\cos\alpha + p\sin\alpha)\frac{\pi a^2 + 2\pi ada - ab}{\sin\alpha} \tag{41}$$

$$\sum V = 0 \rightarrow \mu p\sin\alpha - p\cos\alpha = 0 \Rightarrow \tan\alpha = {}^{1}\!/_{\mu} \tag{42}$$

On simplifying the aforementioned equation (41), by neglecting smaller values and higher order terms, it can be re-written as:

$$\sigma_x\pi a_2 + 2\sigma_x\pi ada + d\sigma_x\pi a^2 - \sigma_x ab = (\mu p\cot\alpha + p)(\pi a^2 + 2\pi ada - ab) \tag{43}$$

Dividing with πa^2 on both sides,

$$\sigma_x\left(1 - \frac{b}{\pi a}\right) + 2\sigma_x\frac{da}{a} + d\sigma_x = (\mu\cot\alpha + 1)\left(2p\frac{da}{a} + p\left(1 - \frac{b}{\pi a}\right)\right) \tag{44}$$

On applying Trescas yield criteria, i.e., p is positive and σ_x will be negative, the induced stress σ_x can be expressed as:

$$-\sigma_x + p = y \Rightarrow p = \sigma_x + y \tag{45}$$

On substituting equation (45) in equation (44), the simplified solution for $d\sigma_x$ can be expressed as:

$$\frac{d\sigma_x}{(y\mu\cot\alpha + \sigma_x\mu\cot\alpha + y)} = 2\frac{da}{a} + \left(1 - \frac{b}{\pi a}\right) \tag{46}$$

Integrating the above equation on both sides:

$$\int\frac{d\sigma_x}{(y\mu\cot\alpha + \sigma_x\mu\cot\alpha + y)} = 2\int\frac{da}{a} + \left(1 - \frac{b}{\pi a}\right) \tag{47}$$

$$\frac{\ln\left(y\mu\cot\alpha+\sigma_x\mu\cot\alpha+y\right)}{\mu\cot\alpha}=2\ln a+\left(1-\frac{b}{a\pi}\right)+c \tag{48}$$

Note: Here, for further simplification considering $\left(1-\frac{b}{a\pi}\right)$ as differential term.

At $a = a_f$, $\sigma_x = 0$, the above expressions become:

$$\frac{\ln\left(y\mu\cot\alpha+y\right)}{\mu\cot\alpha}=2\ln a_f+c \tag{49}$$

$$c=\frac{\ln\left(y\mu\cot\alpha+y\right)}{\mu\cot\alpha}-2\ln a_f \tag{50}$$

Note: The term $\left(1-\frac{b}{a\pi}\right)$ is changes to $\left(1-\frac{b}{a_f\pi}\right)$, at the end of the process.

By putting $B = \mu \cot \alpha$ and substitute equation (50) in equation (48), the σ_x can be estimated as mentioned below.

$$\ln\frac{\left(B\sigma_x+(1+B)y\right)}{B}=2\ln a+\left(1-\frac{b}{\pi a_f}\right)+\frac{\ln(y(1+B))}{B}-2\ln a_f \tag{51}$$

$$\ln\left(\frac{\left(B\sigma_x+(1+B)y\right)}{y(1+B)}\right)^{1/B}=\ln\left(\frac{a}{a_f}\right)^2+\left(1-\frac{b}{\pi a_f}\right) \tag{52}$$

$$\sigma_x=\left(\frac{y(1+B)}{B}\right)=\left(e^{B\left\{\ln\left(\frac{a}{a_f}\right)^2+\left(1-\frac{b}{\pi a_f}\right)\right\}}-1\right) \tag{53}$$

Using aforementioned equations, the analytical solutions for different coefficient of friction are calculated and are shown in Figure 5. The cross validation using FEA-based simulations carried out in subsequent sections.

5 FEM simulation

The analytical closed form solutions are derived and presented in aforementioned sections. However, to substantiate the adequacy of the proposed solution, numerical simulations are found indispensable and are carried out in subsequent sections. As mentioned earlier, the simulations are conducted with ANSYS® platform. The aluminium alloy AA6061 is used as extruded material. The boundary conditions of simulation are kept identical to earlier section. The material properties are tabulated in Table 1. In a similar manner, the constant friction type contact modelling has been carried out between die and billet. The element type such as Solid-285 element (meshing has been shown in Figure 6), boundary conditions (fixed die surface and displacement billet loading surface), simulation environment such as defining adaptive zone to support dynamic meshing and desired loading, and solver configurations remain same. The

steady state solution is used to estimate the results. The step used to achieve steady state solution was 100.

Figure 5 Analytical results for different values of coefficient of friction for different dies having constant extrusion ratio (ER)

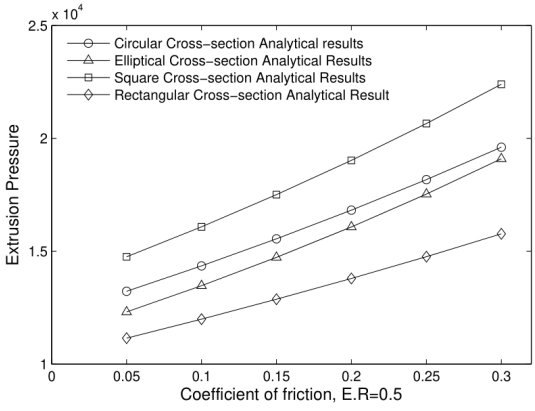

Table 1 Material properties

Density	2,700	(Kg/m^3)
Young's	modulus	61,300(Mpa)
Poisson's	ratio	0.33

Figure 6 Modelling and meshing of components, (a) 3D-model view, (b) front view and (c) isometric view (see online version for colours)

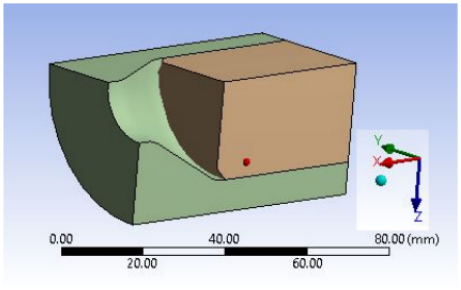

(a)

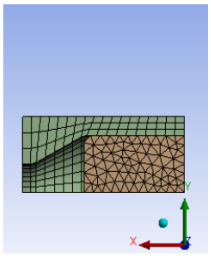

(b)

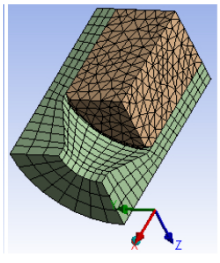

(c)

6 Results and discussion

First the simulations are carried out with constant coefficient of friction such as 0.1. To justify the adequacy of proposed analytical solution, the simulations are also conducted for said shape of dies such as circular, elliptical, square and rectangular sections. The numerically calculated directional deformation, maximum principal stress, and equivalent total strain from simulations are estimated for said dies and are shown in Figure 7. Likewise, the other parameters such as the equivalent total strain and maximum principal stress for different shapes of dies are shown in Figures 8 and 9, correspondingly.

For detailed justification, for circular cross-section, following literature (Ghosh and Mallik, 2010), the maximum pressure estimated from steady state solution are extracted and overlapped with well established analytical solution and are shown in Figure 10(a). From Figure 10(a), one can notice that the simulations approve the analytical results adequately (error ≤ 5%). Then, the maximum pressure observed in simulations for different cross-section of dies are estimated and are shown in Figures 10(b)–10(d) for elliptical, square, and rectangular shapes, respectively. Form aforementioned figures it can be seen that the estimated results from analytical solution agree adequately to numerical simulation results. Moreover, the observed errors are quantified and tabulated in Table 3 and are ≤ 5%, which is satisfactory.

Figure 7 Directional deformation for (a) circular, (b) elliptical, (c) square and (d) rectangular cross-sections (see online version for colours)

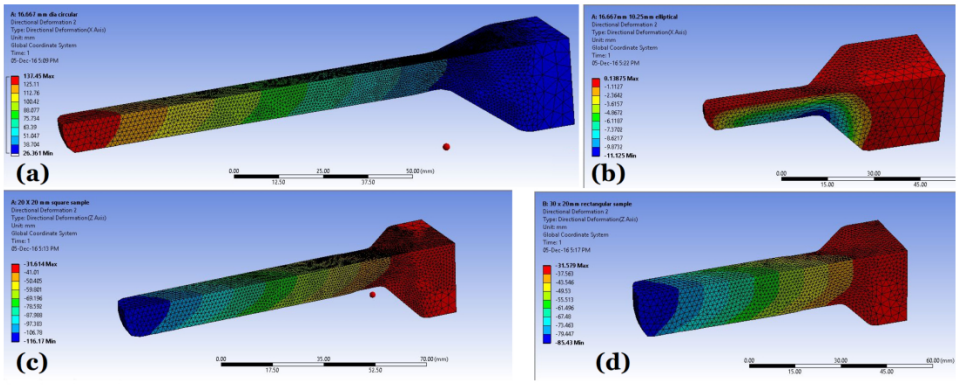

Table 2 Percentage of variation between theoretical/analytical results to simulation results for a constant ER

	Extrusion pressure (MPa)		
Cross-section	*Analytical*	*Simulation*	*Error in %*
Circular (16.667 mm)	21,989.39892	21,593.58974	1.8
Elliptical (16.667 × 10.25 mm)	22,810.62055	22,233.51185	2.53
Square (18 mm)	27,038.23638	26,873.30314	0.61
Rectangle (18 × 12 mm)	17,769.0365	17,7546.9235	1.25

Additionally, the error analyses are carried out to illustrate the performance of simulations. Next, the simulations were conducted for different ERs such varying from 0.2 to 0.8. The observed errors are shown in Figure 11. One can notice from the figure that the analytical results corroborate adequately with simulation result, however, the error rate increases with respect to ER in acceptable range. Subsequently, the investigations are conducted for different contact by varying the coefficient of friction from 0.5 to 0.3. The estimated results from analytical and numerical simulations are shown in Figure 12. It can be inferred from the figure that in a similar fashion, the analytical and numerical results agree to each other with error ≤ 5%.

Figure 8 Equivalent total strain (a) circular, (b) elliptical, (c) rectangular and (d) square cross-sections (see online version for colours)

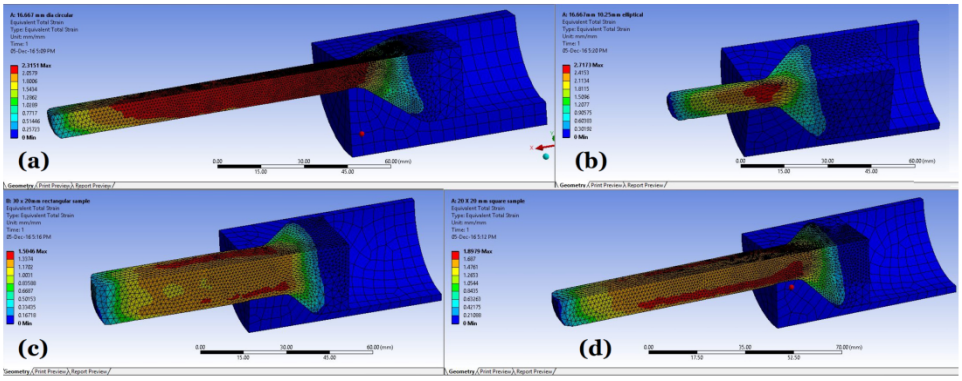

Figure 9 Maximum principal stress and equivalent total strain for (a) circular, (b) elliptical, (c) rectangular and (d) square cross-sections (see online version for colours)

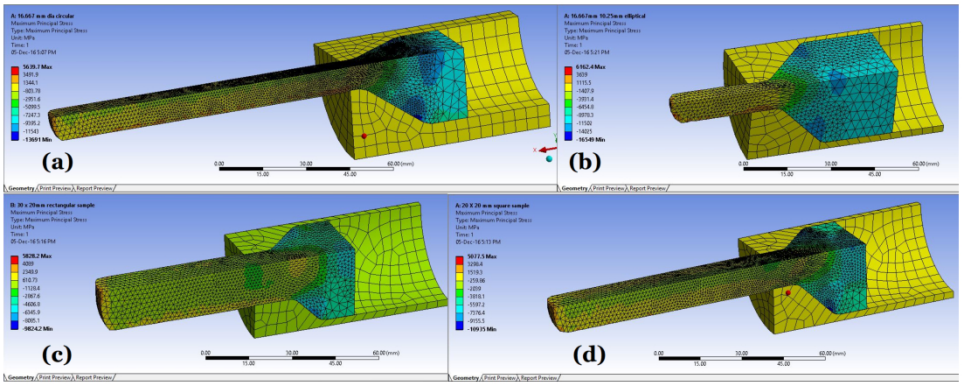

Summarising, the conducted simulations are mimicking of actual direct extrusion process. So, considering all physical boundary conditions are indispensable with appropriate assumptions to attain the accurate results. In extrusion process, material is gone through a large plastic deformation. So, the ER and length (L) to diameter (D) ratio are critical parameters which also depend upon the material properties of the material

under extrusion. The suggested analytical solutions and simulations may be considered as the one which are capable to address the afore discussed lacuna. The demonstrated simulations do not require extreme computational resource. So, it is apposite to examine the real-world direct extrusion process which ultimately cuts the overall cost. The proposed analytical method is also suitable for optimising different process parameters.

Figure 10 Comparison of simulation results against theoretical results for different dimensions of die cross-section, with varying ER (a/b = major dimension/minor dimension)

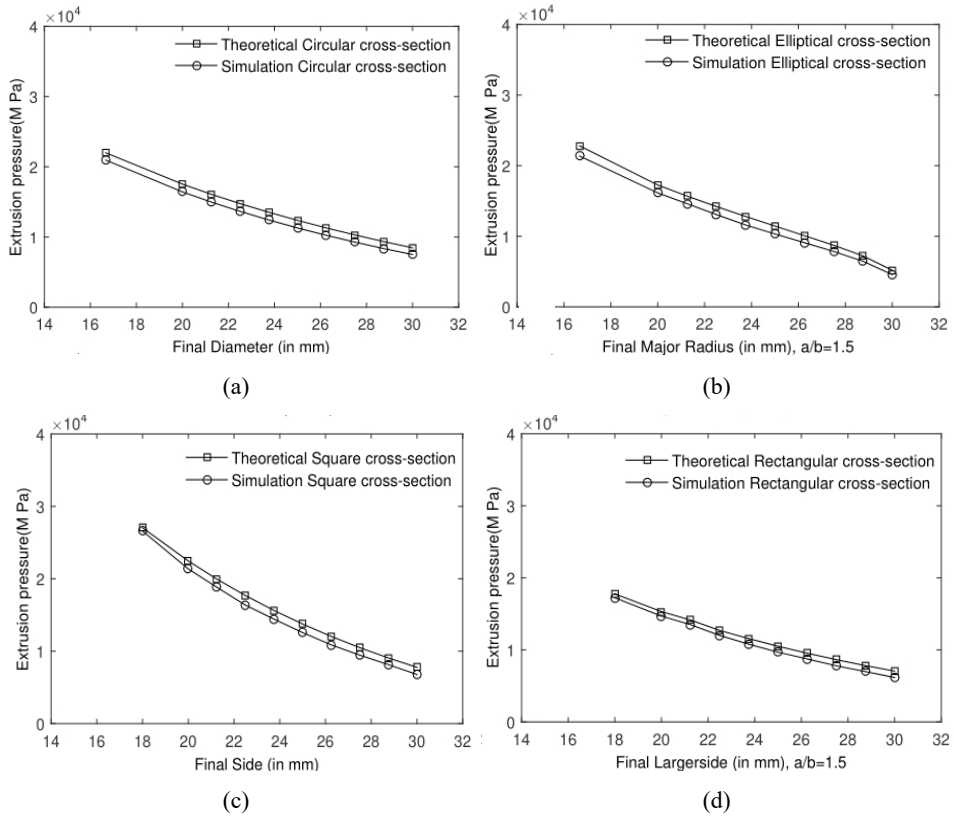

Table 3 Percentage of variation between theoretical/analytical results to simulation results for various cross-sections with varying ERs

Cross-section	*Percentage of variation (%)*
Circular	1.8 to 4.3
Elliptical	2.53 to 4.52
Square	0.61 to 5.05
Rectangle	1.25 to 4.98

Figure 11 Percentage of variation between theoretical/analytical results to simulation results for various cross-sections with varying ERs

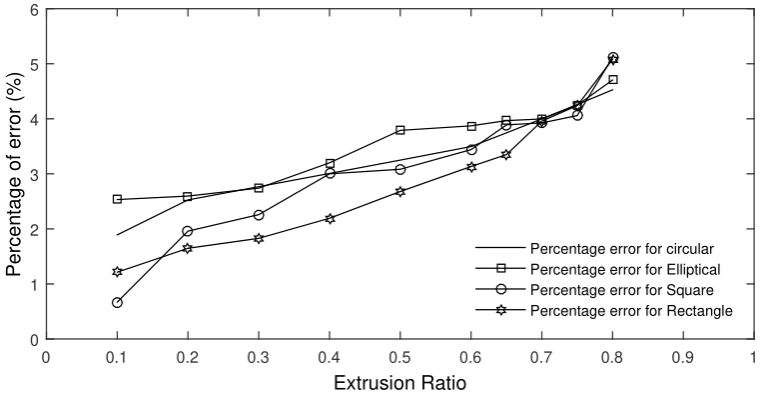

Figure 12 Comparison of analytical results with simulation results for different coefficient of friction and for different dies (ER = 0.5)

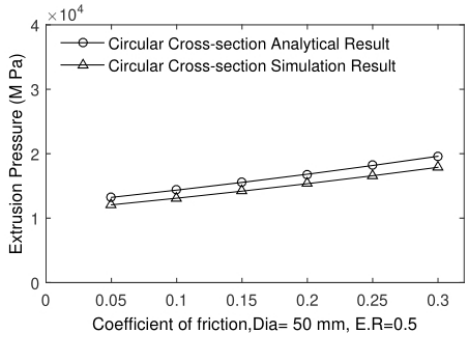

(a)

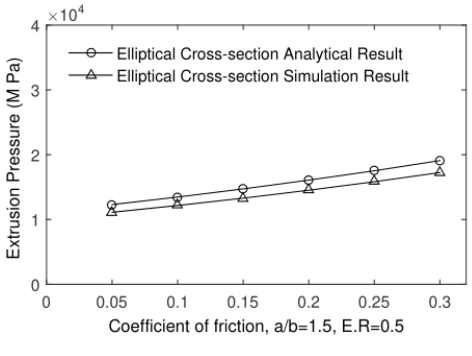

(b)

Figure 12 Comparison of analytical results with simulation results for different coefficient of friction and for different dies (ER = 0.5) (continued)

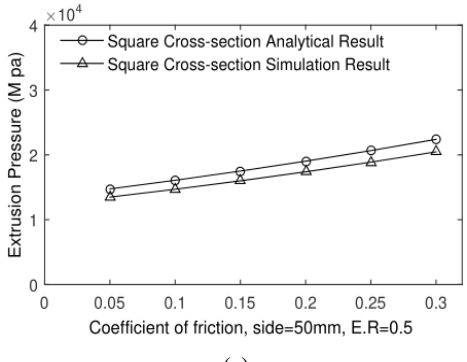

(c)

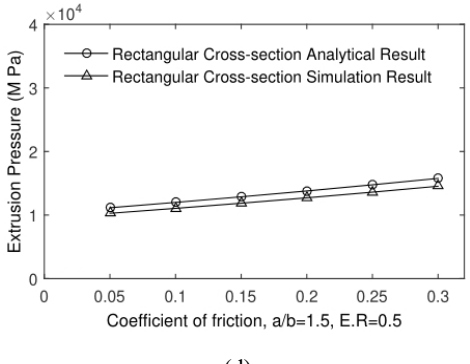

(d)

7 Conclusions

The demonstrated research succeeded in developing analytical model for extrusion with various dies such as dies with elliptical, rectangular and square shapes. Initially the benching numerical simulations are carried out for tensile and compressive tests followed by direct extrusion process using FEA, where the simulation results corroborate with experimental measurements adequately. The detected difference is less than 5%. Then, the analytical solutions for aforementioned shapes of dies are derived and the calculated results are verified with simulation results for constant coefficient of friction. It is noticed from extensive investigations, analytically and numerically, that the extrusion pressure required to extrude the billet varies in ascending order for different cross-sections namely, rectangular, circular, elliptical, and square at any coefficient of friction. Likewise, for the different values of coefficient of friction, the extrusion pressure varies in ascending order for different cross-section namely, rectangular, elliptical, circular, and square. It is observed from above investigations that the numerically calculated results agree to theoretical results with less than 5% of error. The fact of extrusion pressure increases with decreasing ER has also been verified. The reliability of the proposed simulation is observed up to ER 0.8. To the point, the proposed methodologies can be reckoned to evaluate the desired extrusion pressure, suitability of any given material for a given direct extrusion process.

Acknowledgements

The author acknowledges R. Hari Krishna for his support in executing the work.

References

Abrinia, K. and Makaremi, M. (2009) 'An analytical solution for the spread extrusion of shaped sections', *The International Journal of Advanced Manufacturing Technology*, Vol. 41, No. 7, pp.670–676.

Bagherpour, E., Ebrahimi, R. and Qods, F. (2015) 'An analytical approach for simple shear extrusion process with a linear die profile', *Materials Design*, Vol. 83, pp.368–376.

Bathe, K.J. (1982) *Finite Element Procedures*, Prentice-Hall, Englewood Cliffs.

Bauser, M., Sauer, G. and Siegert, K. (2006) *Extrusion*, 2nd ed., ASM International.

Bonet, J. and Wood, R.D. (2008) *Nonlinear Continuum Mechanics for Finite Element Analysis*, Cambridge University Press.

Bressan, J.D., Martins, M.M. and Button, S.T. (2014) 'Aluminium extrusion analysis by the finite volume method', *XII International Conference on Computational Plasticity*, *Fundamentals and Applications*, Vol. 1, pp.1–12.

Bryan, M., Rough, S. and Wilson, D. (2017) 'Flow visualisation and modelling of solid soap extrusion', *Chemical Engineering Science*, Vol. 173, pp.110–120.

Chanda, T., Zhou, J. and Duszczyk, J. (2000) 'FEM analysis of aluminium extrusion through square and round dies', *Materials Design*, Vol. 21, No. 4, pp.323–335.

Chaudhari, G.A., Andhale, S. and Patil, N. (2012) 'Experimental evaluation of effect of die angle on hardness and surface finish of cold forward extrusion of aluminum', *International Journal of Emerging Technology and Advanced Engineering*, Vol. 2, No. 7, pp.334–338.

Comaneci, R., Zaharia, L. and Nedelcu, D. (2015) 'Combining circular-to-rectangular direct extrusion and equal channel angular pressing: Analysis and simulation, *International Journal of Engineering and Material Sciences*, Vol. 22, No. 5, pp.527–533.

Dieter, G.E. (2013) *Mechanical Metallurgy*, 3rd ed., McGraw-Hill, New York.

Frederick, C. and Armstrong, P. (2007) 'A mathematical representation of the multiaxial bauschinger effect', *Materials at High Temperatures*, Vol. 24, No. 1, pp.1–26.

Gadala, M. and Wang, J. (1999) 'Simulation of metal forming processes with finite element methods', *International Journal for Numerical Methods in Engineering*, Vol. 44, No. 10, pp.1397–1428.

George, L.X., Totten, E. and Funatani, K. (2004) *Handbook of Metallurgical Process Design*, CRC Press.

Ghosh, A. and Mallik, A.K. (2010) *Manufacturing Science*, 2nd ed., Affiliated East-West Press Pvt. Ltd., India.

Haghighat, H. and Askar, H. (2015) 'An analytical solution of bimetal rod extrusion process through conical dies', *Gazi University Journal of Science*, Vol. 28, No. 2, pp.301–310.

Khlystov, N., Lizardo, D., Matsushita, K. and Zheng, (2013) *Uniaxial Tension and Compression Testing of Materials*, Tech. rep., MIT University [online] https://web.mit.edu/dlizardo/www/UniaxialTestingLabReportV6.pdf (accessed 2017).

McMeeking, R.M. and Rice, J.R. (1975) 'Finite element formulations for problems of large elasticplastic deformation', *International Journal of Solids and Structures*, Vol. 121, No. 5, pp.601–616.

Noorani-Azad, M., Bakhshi-Jooybari, M., Hosseinipour, S. and Gorji, A. (2005) 'Experimental and numerical study of optimal die profile in cold forward rod extrusion of aluminium', *Journal of Materials Processing Technology*, Vol. 164–165, pp.1572–1577.

Nouri, M., Semnani, H.M., Emadoddin, E. and Kim, H.S. (2018) 'Investigation of direct extrusion channel effects on twist extrusion using experimental and finite element analysis', *Measurement*, Vol. 127, pp.115–123.

Onate, E., Rojek, J., Taylor, R.L. and Zienkiewicz, O.C. (2004) 'Finite calculus formulation for incompressible solids using linear triangles and tetrahedra', *International Journal for Numerical Methods in Engineering*, Vol. 59, No. 11, pp.1473–1500.

Oyinbo, S.T., Ikumapayi, O., Ajiboye, J. and Afolalu, S. (2005) 'Numerical simulation of axisymmetric and asymmetric extrusion process using finite element method, *International Journal of Scientific Engineering Research*, Vol. 6, No. 6, pp.1246–1259.

Pahlevanpour, A., Karparvarfard, S., Shaha, S., Behravesh, S., Adibnazari, S. and Jahed, H. (2018) 'Anisotropy in the quasi-static and cyclic behavior of zk60 extrusion: characterization and fatigue modeling', *Materials and Design*, Vol. 160, pp.936–948.

Plančak, M., Kuzman, K., Vilotić, D. and Movrin, D. (2009) 'FE analysis and experimental investigation of cold extrusion by shaped punch', *International Journal of Material Forming*, Vol. 2, No. 1, p.117.

Quenzi, P.J., Kauppila, R.W. and Weinmann, K.J. (1972) 'Analysis of lateral extrusion of 6061-0 aluminum by slip line theory modified to include strain-hardening, *Journal of Engineering for Industry*, No. 4, pp.971–978.

Ryzinska, G. and Gieleta, R. (2016) 'Experimental and numerical modelling of the extrusion process in 1050a aluminum alloy for design of impact energy-absorbing devices', *Strength of Materials* Vol. 48, No. 4, pp.551–560.

Saboori, M., Bakhshi-Jooybari, M., Noorani-Azad, M. and Gorji, A. (2006) 'Experimental and numerical study of energy consumption in forward and backward rod extrusion, *Journal of Materials Processing Technology*, Vol. 177, Nos. 1–3, pp.612–616.

Sinaie, S. (2009) 'On the calibration of the chaboche hardening model and a modified hardening rule for uniaxial ratcheting prediction', *International Journal of Solids and Structures*, Vol. 46, No. 16, pp.3009–3017.

Tabatabaei, S., Abrinia, K., Tabatabaei, S., Shahabadi, M. and Besharati, M. (2015) 'Analytical modeling of the extrusion process using the electrostatics concept', *Mechanics of Materials*, Vol. 88, pp.87–102.

Yermanok, M. (1997) 'Mechanisms of extrusion of aluminum alloy shapes', *Advanced Performance Materials*, Vol. 4, No. 2, pp.215–221.

Zhang, H., Li, X., Deng, X., Reynolds, A. and Sutton, M. (2018) 'Numerical simulation of friction extrusion process', *Journal of Materials Processing Technology* Vol. 253, pp.17–26.

Zienkiewicz, O. (1967) *The Finite Element Method*, McGraw-Hill Company, London.